COHERENCE PHENOMENA OF MICROWAVE, ELECTROMAGNETIC, AND ELECTRIC FIELDS IN MEDIA AND SAMPLES OF DIFFERENT NATURE

U.Kh. Kopvillem and R.Z. Sharipov

Pacific Institute of Oceanography,
Far–Eastern Branch of the Russian Academy of Sciences, Vladivostok
Received March 18, 1993

A review of experimental studies on microwave, acoustic, magnetic, and electric echo–phenomena in crystalline and amorphous structures is presented. The results of application of electron paramagnetic resonance to the study of self–organization of protozoa are reported. Feasibility of recording of seascape from the dynamics of permittivity of atmospheric layer adjacent to the water surface is demonstrated. Signals of free–field induction and echoes of permittivity produced by biological objects upon exposure to low–power light pulses are analyzed. Our recent data obtained in this line of investigation are reported.

1. INTRODUCTION

In this paper we present in chronological order the experimental facts pioneered by us, which have been investigated or are to be investigated in other laboratories. We hope that apparent heterogeneity of objects, phenomena, and methods discussed here will not embarrass the reader. All the effects being studied here are associated with an interaction between a medium and a superhigh–frequency electromagnetic field with a wavelength of 3 cm. Either pulsed or continuous exposure of the SHF field is analyzed in every particular case. Acoustic, magnetic, and electric coherent states can be excited in the medium depending on the physical properties of a sample or a system. Spatial dynamics of these states in the sample provides a practical application of various effects.

In 1988 an effect of electron spin echo (ESE) in ruby at a frequency of 10^{10} Hz was reported in Ref. 1. It was observed on the $|+1/2> \leftrightarrow |-1/2>$ transition in the sample containing $3\cdot10^{-5}$ at. % of Cr^{3+} ions. In Ref. 1 an important conclusion was drawn that for reliable detection of echo–signal the angle Θ between the static magnetic field $\mathbf{H}_0$ and the trigonal axis $\mathbf{C}$ of a crystal must not exceed 2°. This imposes a very stringent restrictions on conditions of the ESE observation in ruby. Since the system containing Cr^{3+} ions in Al_2O_3 was very promising for the study of various cooperative effects in acoustic and electromagnetic fields, it seemed necessary to perform further experiments on detection of coherent responses.

It is well known in the ESE engineering that a compromise between the sensitivity of a device and its time response characteristics must be reached. Both these characteristics are functions of the cavity Q–factor whose typical value does not exceed 500. This allows one to obtain the sensitivity $N_{\min} \sim 10^{-16}$ cm^{-3} and $\sim 10^{-7}$ s time response in the case of incoherent detection. Such characteristics limit possibilities for performing successful experiments. For this reason we aimed at finding another quantum transition more favourable for the ESE observation in ruby.

A cylindrical crystal was placed inside a tube made of fused quartz. This tube was used as a holder of the sample and an element concentrating the magnetic field component of the SHF field near the tube due to its diamagnetic properties. This results in the increased Q–factor of the sample, whereas the cavity Q–factor remained unchanged.

We were greatly surprised when on the screen of an oscillograph we saw the echo–signal produced by quartz glass upon exposure to two electromagnetic pulses under conditions of zero magnetic field ($\mathbf{H}_0 = 0$). It was the pioneering observation of the echo–signal produced by glass.

2. NONRESONANT EXCITATION OF PHASE MEMORY IN OSCILLATING SYSTEMS

Dynamic phase memory of two–level systems was revealed in 1971 (see Ref. 2). Glass differs from crystal structure by loosely packed atoms and molecules. The vacancies appearing in this packing result in the fact that the relative position of atoms and molecules, which minimizes the potential energy, is no longer unique. In this case glass can be considered as an excited crystalline state with spontaneously disturbed translational invariance. The vacancies result in the fact that many atoms or atomic groups may occupy two equivalent positions having different energy states. The atomic transition between these two energy levels may take place resulting in the formation of the so–called two–level particles.

Such approach to the spatial structure of glass provides an adequate description of specific heat capacity at low temperature, thermal conductivity, and ultrasonic and dielectric absorption. The main contribution to the phase memory of the system comes from a wide spread of natural frequencies of two–level centers. The magnitude of this spread may be equal to the width of the Debye spectrum, i.e., $T_2^* \sim 10^{-12}$ s. Denoting by Δt the duration of an exciting pulse, we obtain at $\Delta t = 10^{-8}$ s that $N_1 \sim NT_2^*/\Delta t \sim 10^{18}$ particles from $N \sim 10^{23}$ particles of a unit volume will respond.

0235-6880/93/07 445-10 $02.00

Spatially two–level particles in glass possess large elastic dipole moments. They are effectively excited by acoustic radiation and generate phonons,[3] because their physical nature is associated with spatial displacements. This displacement is caused by rearrangement of charges in a molecule. Investigations of echoes produced by glass at low and extra–low temperatures show that echoes in the form of sound and electric pulses are peculiar to these spatially two–level particles.

Salient features of the above–discussed phenomenon are the following:

(a) The signal is electrostatic in origin, that is why its maximum is detected at an antinode of electric field inside a measuring cavity.

(b) This effect is observed in zero magnetic and electric polarization fields.

(c) Paramagnetic impurities in some samples are polarized upon exposure to an external magnetic field thereby curbing the activity of spatially two–level particles. This leads to dependence of echo–signal amplitude on the parameters of the external magnetic field.

(d) The echo–signal is well pronounced at a temperature of 4.2 K.

(e) This echo–signal is recorded over a wide frequency range and needs no special resonance conditions.

Based on the idea[4] that the dynamic phase memory is the fundamental property of matter in any state, we systematically sought for various echo–effects in all kinds of substances. As a result, we have discovered the effect referred to as polarization echo (PE) and representing the electromagnetic response of a ferroelectric crystal excited by the electric component of a pulsed SHF field.

Here we discuss only those PE features which are observed in ferromagnetic crystals in the SHF field and have already been observed in our experiments.

Response to two or three pulses has a wide frequency range without typical resonant peculiarities. The echo–signal can be detected only at a temperature of 4.2 K at which the duration of pulses and time interval between them are smaller than some relaxation times. Under certain conditions the echo–signals are repeatedly detected at times 3τ, 4τ, etc (see Ref. 5).

A TE_{112} cylindrical cavity seemed to be very promising for observation of the signal. The signal peaked when the sample was placed at an antinode of electric field. The signal amplitude was much lower inside a coaxial cavity which was usually used for hypersound excitation. This can be explained by the fact that inside a coaxial cavity only a small part of a sample responds while inside a cylindrical cavity the total volume of the sample does. It follows that the echo–signal is produced by the total volume of the investigated sample and that the PE is electrostatic in origin.

The PE has the following salient features:

1. A two–pulse train emitted at times 0 and τ produces the echo–signal at time 2τ. This signal decays as $\exp(-2\tau/T_2)$, where T_2 is characteristic time.

2. In some crystals a three–pulse train emitted at times 0, τ, and τ_1 produces the echo–signal at time $\tau_1 - \tau$. This signal decays as $\exp(-2\tau/T_2)\,[-(\tau_1 - \tau)/T_1]$ (see Ref. 6).

3. The signal amplitudes vary insignificantly in a wide frequency range.

4. The echo–signal is produced by the electric field component.

5. The signal amplitude is several factors of ten higher than that of spin echoes produced by radicals.

6. The signals are independent of static magnetic field if its induction does not exceed 1.2 T (for pure ferroelectrics).

7. The echo–signal amplitude is a function of the angle between the polar axis of a crystal and the electric vector of the SHF field.

8. Only an ordered phase of ferroelectric produces the echo–signal.

9. For powdered sample, the signals from excited hypersonic pulses are no longer detected while the echo–signals of electrostatic origin are still detected.

10. At elevated temperatures $T > 4.2$ K, characteristic times are rapidly shorten and echo–signals vanish.

11. The mechanism of phase memory is associated with spread of natural frequencies of oscillators producing echo–signals.

This physical phenomenon discovered and investigated in Ref. 7 is used for identification of the ordered state of ferroelectrics and investigation of their properties as well as for the development of memory units and signal processing in acoustoelectronics. The objects being studied were chosen from a homologous series of ferroelectrics containing hydrogen and deuterium and having a phase transition temperature of 130 K. In addition, a number of high–temperature ferroelectrics were investigated.

Since shaping of the PE is closely related to the process of sound generation, it is of interest to study the effect of the static electric and magnetic field characteristics on the parameters of echo–signal and process of sound generation. Direct relationships between the crystal quality and PE characteristics were experimentally determined.[9] The echo–signal is not produced by perfect crystals with a single magnetic domain, for example, by $LiNbO_3$ crystals which are commonly used for a second–harmonic generation in lasers. This is due to the absence of inhomogeneous broadening described by the term $1/T_2^*$. Any structural disruption (polydomain structure and exposure to a high–gradient static electric field) engenders broadening and produces echo–signal.

Bearing these circumstances in mind we investigated ferroelectric crystals with impurities such as $LiNbO_3 : Fe^{3+}$, $LiNbO_3 : Ni^{2+}$, $LiNbO_3 : Co^{2+}$, and $LiNbO_3 : Cu^{2+}$. This allows us to make use of the ESE method. The ESE signal is well pronounced at low ion concentration because the rate of paramagnetic relaxation in the system containing electrons with spins is proportional to the ion concentration. At the same time, simultaneous observation of the PE is difficult due to a small value of the parameter $1/T_2^*$ of the electric dipole system. The enhanced ion concentration results in much smaller relaxation times and hence in vanishing spin echo. In this case the PE signal becomes well pronounced.

On this basis we performed a number of experiments aimed at detection of the PE in a static magnetic field. In this paper we present a minute description of the results obtained in a $LiNbO_3 : Fe^{3+}$ crystal with the ion concentration of about 0.05%. Magnetic field was applied parallel to the optical axis of the crystal. In the sample we observed multiply reflected decaying pulses produced by a running hypersonic pulse initiated by a single SHF pulse. Exponentially decaying trailing edge of these pulses characterises the background attenuation of sound radiation at the excitation frequency. It decreases by about 10 dB in the magnetic field with a magnetic induction of 0.12 T. In addition, we measured the PE as a function of the magnetic field strength and measured its relaxation time T_2. Variation of the parameter T_2 with increasing magnetic field strength indicates intimate relationship between the PE and

the acoustic Q–factor of the sample as well as inverse proportionality between T_2 and attenuation coefficient of sound radiation. Since the paramagnetic impurities are the centers of dislocations in the crystal, these observations point out the mechanism of coupling between dislocations and paramagnetic impurities. This can lead to polarization of dislocations in the magnetic field and large variation of sound radiation absorption due to dislocations.

The magnetic field influences not only absorption of hypersound but also shaping of the PE associated with inhomogeneous broadening or phase relaxation caused by interactions of dislocations. Such interactions can be considered to occur between line bent dislocations within the scope of the Frenkel–Kontorova model. If we restrict our consideration to pairwise interactions, we may assume that two bent dislocations form stably coupled structures referred to as breathers.[10]

The crystal can be treated as a thermostat containing the dislocation gas. In this case the thermodynamic subsystem of breathers whose oscillation frequencies spread exists in this crystal. This spread of frequencies is engendered by inhomogeneous broadening with allowance for the interaction between breathers and phonons of a lattice. The role of the first pulse in shaping of the PE is to form the coherent state of breathers in this crystal. In this case condition $\Delta t < T_2^*$ must be satisfied, where Δt is the pulse duration and T_2^* is the time of reversible phase relaxation. Coherence implies that all breathers oscillate in phase. Interaction of breathers with phonons results in their dephasing after the pulse has ceased. Superposition of the second pulse reverts the phase relaxation. In such a manner the classical mechanism of echo–signal shaping is formed in which the only assumption is introduced that the echo–signal is produced by oscillations of pairwise line bent dislocations possessing the elementary electric dipole moments.

We also investigated the effect of parameters of the static electric field on the characteristics of hypersound radiation during its propagation through a pure $LiNbO_3$ crystal having a single magnetic domain. Polarization of this crystal with dislocations, being electrostatic in origin, also takes place in this field. Its characteristics are analogous to the above–discussed. In our case the acoustic energy losses due to propagation are minimized for the electric field strength $E_0 = 10^4$ V/cm applied perpendicularly to the optical axis **C** of the crystal. Since the dislocation structure of each crystal belonging to the same class is individual, effect of minimization of acoustic energy losses takes place for different values of E_0.

Effect of a radio–frequency electric field results in modulation of exponential decay of the PE. The degree of modulation depends on the field strength. Resultant oscillations are engendered by modulation of energy spectrum of the centers initiating the PE signal. Theory of this effect is well developed for systems with spins and can be employed for oscillating centers. We observed this effect in a $LiTaO_3$ crystal having polydomain structure. All the results described here were reported in details in Refs. 1–12.

At the end of this Section we give the results obtained by Zverev[13] for sand of volcanic origin which covers beaches of volcanic islands. The samples were collected at the foot of Mendeleev volcano in Kunashir island. This object was unique in composition of sand containing 80% of pyroxene, 3% of ferric hydrate, 3% of martite, 2% of amphibole, 2% of olivine, and grains of various rocks. This allowed us to study separately its different fractions with the use of appropriate technology. As a result, we observed the PE in volcanic sand without quartz and magnetic fractions, i.e., in a fraction with minimum magnetoelastic and electroelastic nonlinearities required for production of the PE. A single–pulse PE typical of the ordered antiferromagnetic state of the medium (see Fig. 1) was recorded.

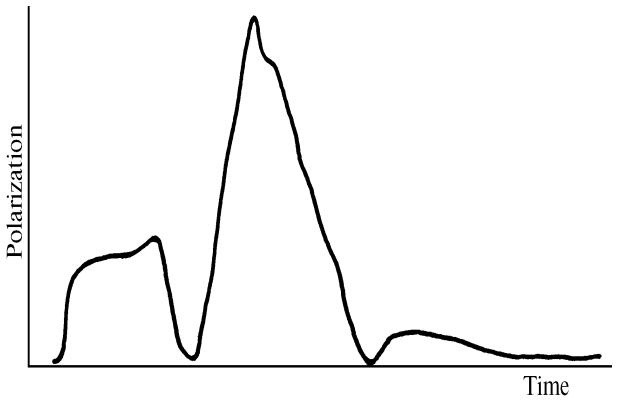

FIG. 1. A single–pulse radio–frequency echo from volcanic sand.

The echo was detected in the frequency range 13.25–15.5 MHz. As the pump intensity rises, echo–signals increase following oscillating echo pattern. Moreover, the signal amplitude is integrated when the number of pairwise exciting pulses increases. The signal amplitude increases over the course of 2 s to a fixed limited value at a 100–Hz repetition frequency of these pairwise pulses. Then the echo–signal collapses to its initial value. These effects of signal integration and collapse disappear as the repetition frequency decreases to 1–10 Hz. For refined sand the echo–signal amplitude diminishes, and shorter radio–frequency pulses are required to reproduce the echo–signal. Induction–induced signals were observed at room temperature while echo–signals – only at a temperature of 77 K. The signal vanishes after shaking up or rotating the sample. To reproduce the echo–signal, it was necessary to search for new resonance conditions by way of frequency scanning and matching the phase of a radio–frequency pulse carrier. This effect was observed in an inductance coil of working circuit and was most pronounced in an electric field of a capacitor. The detected echo depends on the temperature, chemical composition and structure of samples, and method of excitation. For these reasons it is a valuable tool for geo– and physical studies. For the most part these experiments were carried out under the field conditions.

2. ELECTRON SPIN ECHO IN RUBY

In this Section we will discuss the results of our studies on echo–spectroscopy of magnetic systems localized within crystalline structures of leucosapphire. We studied $Al_2O_3 : Cr^{3+}$, $Al_2O_3 : Fe^{3+}$, and $LiNbO_3 : Fe^{3+}$. However, it will suffice to focus on the data obtained for Cr^{3+} ions localized within Al_2O_3 in the sense that more delicate choice of experimental conditions is required for this object. The other above–enumerated objects present no difficulties for echo–signal observation. Moreover, ruby suits best for studying cooperative effects under conditions of superposition of different fields, for example, electromagnetic and acoustic fields.

As it has already been pointed out, in our pioneering experiments with ruby we determined the conditions of

detection of electron spin echo (ESE). Having analyzed the available data, we arrived at a conclusion that quantum transition $3 \leftrightarrow 4$ is most suitable for echo observation in the field with magnetic induction $H_0 \sim 0.54$ T applied at the angle $\Theta = \pi/2$ relative to the optical axis. Indeed, in monocrystal of $Al_2O_3 : Cr^{3+}$ we detected the ESE at a frequency of $9.56 \cdot 10^{-9}$ s^{-1} for a chromium ion concentration of about $3 \cdot 10^{-4}$. In contrast to the available data, we pioneered the detection of echo–signal in ruby with such a concentration of active impurities. It was demonstrated that the fluctuations in nuclear magnetization did not distort an envelope of echo–signal decay for perpendicular orientation of the static magnetic field **H** relative to the optical axis **C** of a crystal. Experiments were performed for extremely low concentration of chromium ions comprising about $3 \cdot 10^{-6}$. In this case echo–signals were recorded for all quantum transitions and $\mathbf{H} \parallel \mathbf{C}$, while for $\mathbf{H} \perp \mathbf{C}$ the ESE was also recorded at a temperature of 77 K. All measurements were performed for samples with plane–parallel polished ends. This allowed us to use them in experiments with hypersound fields. Rods made of crystalline quartz together with piezosemiconducting films made of CdS were used as sound generators. A transducer consisting of such an element was placed at an antinode of electric field inside of a measuring cavity. These experiments were performed later on.

It should be noted that in contrast to the perpendicular orientation $\mathbf{H} \perp \mathbf{C}$, for $\mathbf{H} \mid \mathbf{C}$ the echo–signal decay vs. exciting pulse interval was oscillating in nature. This is due to a superfine interaction (SI) of a paramagnetic ion with its close surroundings formed by magnetic moments of nuclei. The same modulation of the ESE decay was observed in $Al_2O_3 : Fe^{3+}$ for arbitrary orientation of the magnetic field $\mathbf{H}_0$ relative to the axis **C**. The signals were recorded for any transition of Fe^{3+} ions. In $LiNbO_3 : Fe^{3+}$ modulation was not recorded. This may be the reason why a crystal exhibits piezoelectric properties which give rise to elastic wave field after termination of each acting pulse. This field forms a new channel for cross relaxation processes but the SI slows down.

It is well known that for most comprehensive interpretation of modulation structure of the ESE decay the configuration of closest surroundings of ion must be known as well as effect of its more distant neighbors. Effect of crystalline cores of nuclei on paramagnetic ion can be experimentally investigated when it is exposed to the appropriate radio–frequency field matched with the static magnetic field strength. Thus, one can proceed to experiments on pulsed double electron–nucleous resonance. In addition, it should be kept in mind that complete excitation of electron paramagnetic resonance (EPR) spectrum is difficult to obtain in experiments on the ESE, and hence it is studied under conditions of partial excitation of this spectrum. All these points were covered in ample detail in Ref. 14. Our results were presented in Refs. 5 and 15–17.

3. DETECTION OF SPIN LABELS OF PROTOZOAN SELF–ORGANIZATION THROUGH THE EPR

According to a general idea of highly non–equilibrium physical phenomenon, we assume that any biological self–organizing system dies in the following manner: its bias from equilibrium increases up to a certain critical point followed by avalanche–type decay of this state. The typical features of this phenomenon are generalized in the notion of avalanche[18] the theory of which describes the decay of an arbitrary highly non–equilibrium state of a given physical system. We have found one of the possible parameters of this process, namely, the forbidden line of the EPR of Mn^{2+} ion in noctilucous plankton. This line can be used to measure the parameter of axial intramolecular crystalline field in living plankton. This field varies synchronously with avalanche–type decay describing the manner of dying of noctilucous plankton. This type of plankton is rare in coastal water; however, its large schools appeared for unclarified reasons in the Gulf of Peter the Great in spring of 1988. This provided us a basis for its experimental application.

Poisoning of plankton with Mn^{2+} ions was indicated through observation of the EPR spectra of Mn^{2+} ions assimilated by plankton up to the critical value of concentration C_c. We determined the constant of spin Hamiltonian D of ion in noctilucons plankton from the EPR spectrum. In such a way temporal behavior of the value $D(t) \equiv P(t)$ can be inferred, where P is a certain cooperative parameter describing the evolution of avalanche. This experiment (active EPR) differs substantially from the traditional EPR on Mn^{2+} ions in various media (passive EPR) in that the Mn^{2+} ions yield the information about statics and dynamics of a medium with the given physical properties in the case of the passive EPR while in this case a medium exhibits a ramified system of feedback loops which are responsible for temporal evolution of the system properties under the action of self–regulation of an organism.

In our studies we employed three procedures of interaction $Mn^{2+} \leftrightarrow$ plankton:

1. Small crystals of salt $MnCl_2 \cdot 4H_2O$ were thrown into the samples containing plankton. These samples were collected from the sea water with the use of a plankton gas–type net. The result was observed through a microscope at 100X magnification (its field of view was about 0.3 cm^2) with variable focal depth. Typical size of noctilucous plankton was $\sim 10^{-2}$ cm. We could visually observe the dependence of lifetime of individual noctilucous plankton on its separation from the salt crystal.

2. Salt $MnCl_2 \cdot 4H_2O$ was dissolved in sea water and this solution was added to a sample containing living plankton. In this case we failed to detect the penetration of Mn^{2+} ions into the organism of noctilucous plankton by the EPR method. It is believed that starting with a certain nonfatal concentration of Mn^{2+} ions in sea water $C \ll C_c$, they form such complexes with diamagnetic salt which can hardly penetrate through a membrane of noctilucous plankton.

3. Salt $MnCl_2 \cdot 4H_2O$ was dissolved in distilled water, and then this solution was added to the sample containing living plankton. In this case we detected the penetration and combination of Mn^{2+} ions within the organism of noctilucous plankton by the method of the EPR on Mn^{2+} ions and the fatal concentration of Mn^{2+} ions in this solution C_{fc} was much less than C_c. This means that in distillate Mn^{2+} ions form complexes which can easy penetrate into the noctilucous plankton organism and combine with macromolecules there. This phenomenon is referred to as effect of Mn^{2+} penetration through a membrane.

Thus we have found the forbidden line of the EPR of Mn^{2+} ion indicating the penetration of Mn^{2+} ion into the organism of plankton and ion combination with macromolecules in this organism. It is important that the parameter of intramolecular axial electric field describes

dynamics of self–organizing biological system. It has been found that plankton enriched with Mn^{2+} ions dies in the manner of boson avalanche.

Below we try to show that Cd^{3+} rare–earth ion is an effective paramagnetic probe for the study of self–organization. The information about surroundings and conformation rearrangement of biological complex formed by a living system and Cd^{3+} ion is contained in the evolution of the fine structure of the EPR of the ion. To study the fine structure of the EPR of Cd^{3+} ion in protozoan, we use zooplankton *euphausia superba*. Distillate containing 3% of $CdCl_3$ was added to 0.25 ml of sea water containing zooplankton *euphausia superba* in a 1 : 3 ratio. On the average, 10–15 individuals with the size $0.5 \le l \le 2$ mm were studied. It took only 0.5 min to place a capillary tube filled with the sample inside a cavity. The EPR spectrum was recorded with the RE–1308 spectrometer at once and in an hour and 15 hour intervals after the sample was placed in the cavity at a temperature of 25°C (the sample was thermally stabilized). At the first stage for $\Delta t \le 1$ h the self–organization intensifies, and this is accompanied by the increase of the constant D. Further zooplankton dies, after $\Delta t \le 15$ h Cd^{3+} ions are completely separated from macromolecules, and the parameter D takes the value typical of water solutions of salt $CdCl_3$.

Thus it was shown that rare–earth Cd^{3+} ion is an effective paramagnetic probe for the study of self–organization. The axial D and rhombic E parameters of the fine structure of biocomplex were determined from the EPR spectrum of combined ion. The variation in these parameters determined by self–organization was recorded. Additional transitions corresponding to a superfine structure of Mn^{2+} ions were distinguished from the background fine structure of the EPR of ion for critical concentrations of Cd^{3+} ions. The synergistic character of interaction of ion with self–organization system of living organism was inferred in Refs. 19–21.

4. THE EPR AND JEAN–TELLER EFFECTS IN SUPERPARAMAGNETIC CLUSTERS OF MARINE BOTTOM SEDIMENT AND ROCK

Non–trivial magnetic properties and relaxation processes in superparamagnetic (SP) particles can be effectively studied by the EPR method. Its application to the study of finely dispersed particles of natural origin is of pressing interest. In this Section we present the results of the study of individual particles encountered in marine bottom sediment and rock of the mountain Belukha of Central Altai by the EPR method. The objects under investigation represent an ensemble of finely dispersed particles combined in clusters by action of magnetic forces. This cluster appears to be inserted in a matrix made up of aluminic and silicic oxides. In rock these clusters are surrounded by alumino–silicate in the form of octahedron with monoclinic imperfection. The size of these clusters is no more than 0.1 mm. There is reason to believe that they are volcanic in origin.

Their behavior in magnetic field is characterized by abrupt changes of the vector of total magnetic moment between the directions of the axes of easiest magnetization. Under these conditions the magnetic moment diffuses over a solid angle in a potential field of magnetic anisotropy. The processes of establishing the equilibrium magnetization are well pronounced in the spectra of the EPR of the SP particles (see Fig. 2). On the segment AB the ensemble of magnetic moments of the SP particles is in non–equilibrium state upon exposure to the electromagnetic and variable external magnetic fields. This state associated with magnetization fluctuations lasts until the directions of magnetization and external magnetic field become parallel. The study of relaxation processes in non–equilibrium system is always of interest. These processes are characterized by abrupt change of the static external magnetic field strength from H_1 to H_2 (Fig. 3). In this experiment relaxation of magnetic moments of the SP particles involves two processes, namely, fast and slow ones. First, the local equilibrium inside separate potential wells of magnetic anisotropy is fast established, then populations in the vicinity of different axes are gradually flatten through rare but fast transitions, and the system attains its equilibrium. In addition, the slow process has the modulated structure characterizing magnetic interaction of the net moment with surroundings.

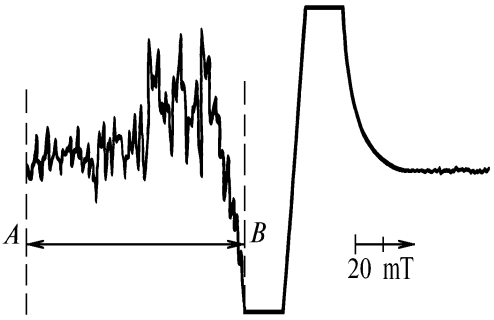

FIG. 2. The EPR spectrum of supermagnetic particles of marine bottom sediment. Fast fluctuations of magnetization can be seen on the segment AB.

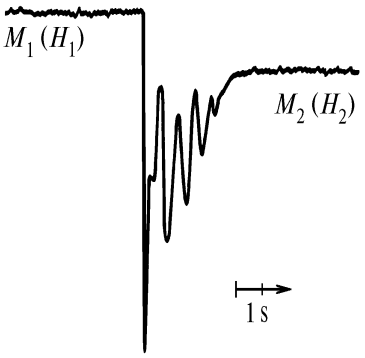

FIG. 3. Relaxation of magnetization after abrupt change of magnetic field strength. Here $M_1(H_1)$ and $M_2(H_2)$ are the magnetization in the fields H_1 and H_2.

Temperature dependence of magnetization for fixed magnetic field strength on the segment AB is shown in Fig. 4.

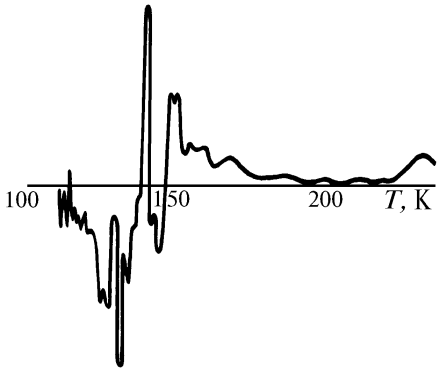

FIG. 4. Magnetization vs. temperature.

Electron microprobe analysis indicates that these particles involve the following complexes: Al_2O_3, Na_2O, K_2O, SiO_2, FeO, MgO, CaO, MnO, TiO_2, and Cr_2O_3. The weighting coefficients are highest for Al_2O_3, SiO_2, and FeO and equal to 0.13, 0.215, and 0.279, respectively. For this reason we state that all magnetic oscillations and other anomalies owe their origin to Fe^{2+} ions. It is well known that supermagnetic behavior is observed in the systems with particles of size < 100Å [a powder of Ni in SiO_2 and Al_2O_3 (see Refs. 22 and 23)]. Moreover, it is known that Fe^{2+} ions in ligand surroundings with lower symmetry are the Jean–Teller systems. The Jean–Teller effect is usually associated with orbital degeneration of electronic state initiating vibratory interaction with unsteady configuration of atomic lattice. In our case there is magnetism in which this lattice makes no significant contribution. However, exchange interactions, when the lattice is subject to action, induce structural transitions and conversely, any action on the lattice may lead to pronounced fluctuations of the exchange forces. In these compounds many anomalous properties are manifested, such as anomalous temperature dependence of magnetic moment associated with structural phase transitions, fluctuation of the parameters in external magnetic field, and so on. In magnetics containing ions with orbitally degenerated ground state the coupling of the orbital structure with multipole order results in the above–described effects which are experimentally observed. A magnetic field applied to the object affects simultaneously the orbital magnetic moment and spin system. For this reason the dependence of the magnetic moment on the magnetic field strength becomes nonlinear. The abrupt changes of magnetization on the segment *AB*, which can be seen on the spectra (Fig. 2) between various magnetic and orbital structures, can be explained by this fact. The abrupt change of the magnetic moment with field strength implies the manifestation of metamagnetism in the process of exchange interaction. It is precisely this process which explains, in our opinion, the temperature dependence shown in Fig. 4. These transitions associated with temperature fluctuations of magnetization clearly demonstrate the dynamic Jean–Teller effect.

In conclusion let us name one more positive property of magnetics, namely, magnetic anisotropy (Fig. 5). A propeller shown in this figure illustrates variations in the amplitude of abrupt changes of magnetization as functions of the angle of the vector of net magnetic moment with respect to the vector of the magnetic field strength. All the objects considered above possess spontaneous magnetism which can be easily measured by the EPR technique. Figure 6 shows an example of measuring of initial magnetization by this technique. Here we have presented not all unique physical properties revealed by us in these objects but the part of them which requires no new approaches to the interpretation of this phenomenon. Some data were reported in Refs. 24–26.

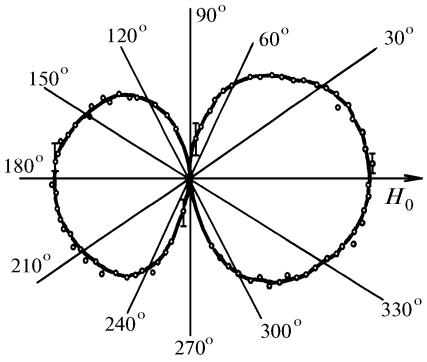

FIG. 5. Angular dependence of magnetization.

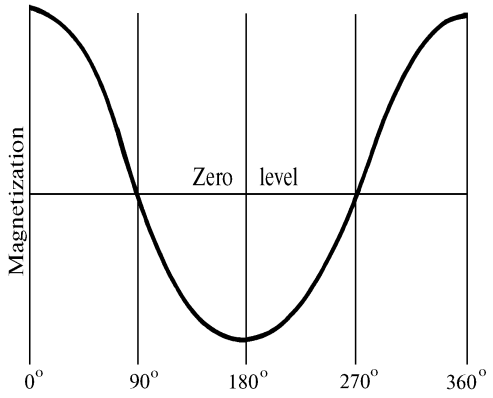

FIG. 6. Measuring of spontaneous magnetization.

As a rule, the effect of magnetic dipoles on the behavior of a quantum system is less pronounced than effects associated with electric dipoles. Thus magnetic dipoles can be compared in strength with electric quadrupoles, magnetic quadrupoles – with electric octopoles, and so on. Bearing this in mind we concluded that electric characteristics of the medium yield the information not less important than magnetic characteristics. The main electric parameter describing the internal dynamic processes in the medium is the permittivity ε. By measuring permittivity in dynamic regime we obtained some results for a number of examined media. These results, in our opinion, are of interest for the reader.

5. TOMOGRAPHY OF THE ATMOSPHERE ADJACENT TO THE OCEAN SURFACE FROM ITS PERMITTIVITY

Measurements of permittivity of the atmospheric layer adjacent to the water surface were performed by resonance technique from aboard the scientific–research vessel *Professor Bogorov* in 1988. They were aimed at: (1) investigation of spatio–temporal variations of permittivity near the water–atmosphere interface and (2) determination of permittivity as a function of the basic meteorological parameters involving more complicated formations such as molecular conglomerations and suspensions. Permittivity of the atmospheric layer adjacent to the water surface was measured with a device based on the Krein two–cavity interference refractometer. Scheme of the device included two channels, namely, the reference channel with evacuated cavity and measuring channel with open cavity. Simplified block diagram is shown in Fig. 7. The instrumental complex was located at the laboratory. Air was sampled on the upper desk through a rigid PVC plastic pipe. It was pumped into the working cavity by a compressor. Measurements were performed in sailing and at rest with an accuracy better than 99.9%. Measurements performed in the Pacific and Indian oceans yielded interesting information about the correlation between ocean dynamics and permittivity of the atmospheric layer adjacent to the water surface. This correlation may be used to describe an interaction of the ocean with the atmosphere on the molecular level.

The regions of underwater ridges in the open areas of the global ocean with special hydrodynamic and biological conditions attract the attention of oceanographers. For example, in the Pacific ocean on November 21, 1988 the effect of "entrainment" of the refractive index or permittivity by the seascape of the mountain Kagoshima, whose top was located at 35°48′ N, 144°20′ E, was discovered. Dash line in Fig. 8 shows the seascape of the mountain and dots indicate the reflection coefficient of the

atmospheric layer, in relative units, averaged over a 2 min interval. Local time aboard the vessel is plotted on the abscissa. Elevation of the mountain above its foot was 4150 m, and its top was nearly 1650 m below the ocean surface.

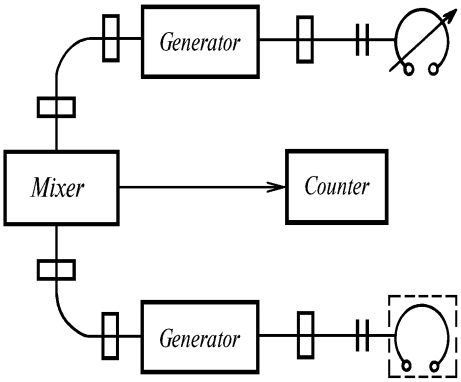

FIG. 7. Block diagram of the permittivity meter.

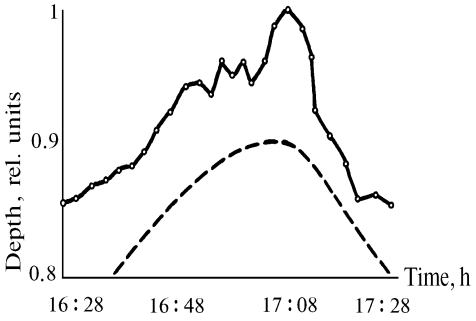

FIG. 8. Effect of entrainment of permittivity of the atmospheric layer adjacent to the water surface by the seascape of the mountain.

It is well known that eddies are continuously produced in the regions of interaction between ocean streams and underwater ridges. For this reason the anomalous depth behavior of temperature and salinity is observed in the water column above the tops of these ridges. Hence the effect of entrainment of the refractive index or permittivity of the atmospheric layer adjacent to the water surface is due to rising of deep water to the surface. Owing to such a rise the temperature of the surface water drops and vapor above the water surface condenses thereby resulting in a higher value of permittivity of the atmospheric layer. Moreover, the regions of underwater ridges may possess energy resulting in large emission of water droplets into the atmosphere.

Let us point out some most interesting results obtained with the help of this device.

1. Recording of the seascape to depths as great as 2 km from variations in permittivity near the ocean surface.

2. Establishing of the spectrum of permittivity fluctuations in the atmospheric layer adjacent to the ocean surface along the 10000–mile path. The amplitudes and frequencies are functions of time and geographical location and can be employed to compile the maps of a new type. These maps describe analytic and dynamic peculiarities of maritime regions. The fluctuations and changes of permittivity of the atmosphere are primarily caused by the molecules, clusters formed from the water molecules, and other atmospheric inhomogeneities involving biological impurities.

3. Detection of 5–min periods of oscillations in the spectra of permittivity in the atmospheric layer above the water surface which are typical of the sun.

Hence permittivity of the air layer adjacent to the ocean surface turns out to be the important oceanographic parameter and can be used in practice among other oceanographic parameters such as temperature, pressure, salinity, sound speed, and absorption coefficient of acoustic radiation. Finally, permittivity can be the valuable dynamic parameter for monitoring of the state of the global ocean, earth, and environment. It can serve as one of the predictors of natural disasters such as tsunami and typhoon. The electric dipole strengths and resonance frequencies of the system play important roles. The contribution of the biosphere to permittivity of the atmosphere can be evaluated.[27–29]

6. COHERENCE PHENOMENA IN BIOLOGICAL OBJECTS SUCH AS LOW–FREQUENCY OSCILLATIONS OF PERMITTIVITY AND ITS INDUCTION AND ECHO STIMULATED BY LOW–POWER LIGHT FLUX

In this Section we discuss some physical properties of living systems found by measuring of permittivity in dynamic regime. Measurements were carried out with a dual channel microwave refractometer described above. Investigated biological object was placed in one arm involving a working cavity, another arm was evacuated. After the reference and information–bearing signals interfered, the measurable parameter was recorded with an error no more than 0.1%.

We investigated a wide variety of biological objects with different levels of organization. *In vitro* experiments were performed with red and green uni–cellular algae, mould, and yeast. *In vivo* experiments were performed with *blattella germanica* and *muska domestica*. A fragment of *in vitro* recording of permittivity oscillations for *in vitro* experiments is reproduced in Fig. 9. The deviations of permittivity from a certain fixed level are plotted on the ordinate and time is plotted on the abscissa. When the test specimen is absent in the working cavity, the output straight line is always recorded which corresponds to the constant permittivity.

An example of *in vivo* recording with corresponding object is shown in Fig. 10. We believe that overshoots characteristic of the curve are responsible for biorhythms of the object located in the measuring cavity and reflect its vital activity. By comparing this record with Fig. 9 in which the curve describing the behavior of permittivity resembles a noise track, we can conclude that in this case we are dealing with an ensemble of uni–cellular algae or yeast cells. In this ensemble the vital activity shows no evidence of coherence, that is why the record has such a form. By taking the Fourier transform we reveal a set of long–period variations of permittivity in the spectrum of biorhythms shown in Fig. 10. The common period for both biological species is equal to 27 s. It is possible that this period is versatile and represents a certain constant for all living systems.

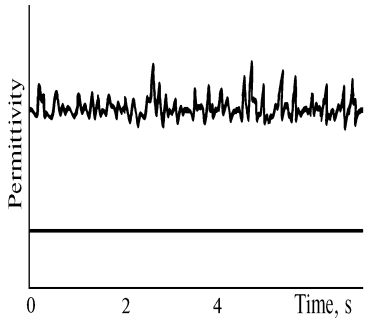

FIG. 9. Spectrum of permittivity fluctuations measured in vitro.

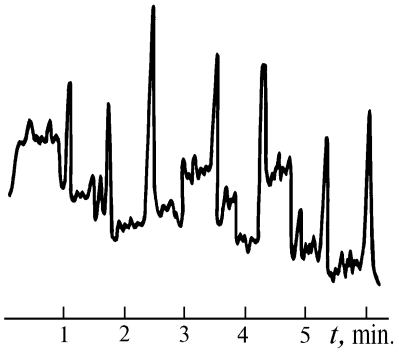

FIG. 10. Biorhythms of blattella germanica measured in vivo.

After recording of the signals of vital activity a problem arose on assessment of the sensitivity of the above–mentioned objects to an external weak excitation. Experiments with low–power light flux passing through a light guide and incident on the test specimen were performed. The intensity of this flux of short duration was 0.2 mW/cm^2. In all experiments we recorded light–induced signals of permittivity. These signals characterize dynamic processes in the system of electric charges upon exposure to light. The objects placed in the measuring cavity were illuminated by coherent or incoherent light. A He–Ne laser was used as a source of coherent light, and an incandescent lamp – as a source of incoherent light. The signals of free induction and echo after single–pulse illumination are shown in Fig. 11, while Fig. 12 illustrates the signals produced after two–pulse illumination. In the latter case we observed two–pulse echo.

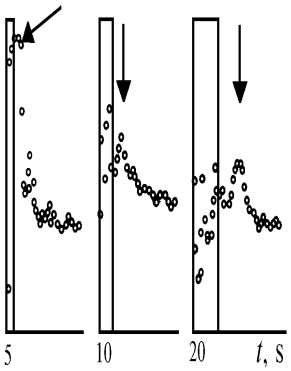

FIG. 11. Signals of induction and single–pulse echo of permittivity (shown by arrows) initiated by low–power light flux. The object is blattella germanica.

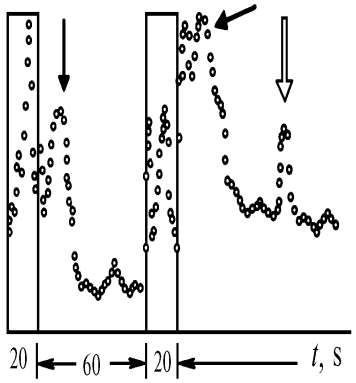

FIG. 12. Single– and two–pulse echo–signals of permittivity.

Let us enumerate the basic properties of these signals.

1. We did not observe the echo–signal decay in accordance with the well–known formula $A_e \sim A_0 \exp(-m\tau/T_2)$, where m is the coefficient, τ is the interval between illuminating pulses, and T_2 is the characteristic time for electric charges.

2. The period of observation of two–pulse echo–signal attains several minutes.

3. The signal amplitude and shape are not explicit functions of light exposure time.

4. The start of two–pulse echo–signal is recorded at the instant which is somewhat different from 2τ peculiar to the known types of echo phenomena.

5. The envelope of the decaying signal of free induction and echo–signal shape have the complicated forms.

6. By comparing the data on coherent and incoherent light illumination we did not find noticeable differences in intensities, durations, and envelopes of the signals.

Based on the last property, we may conclude that the leading and trailing edges of illuminating pulse produce single–pulse echo and represent a trigger for fast overthrow of electron from one state to another. Each electron transition is accompanied with slow conformational transitions. In this way nonlinear properties initiating the above–described signals have their origin in electron–conformation interactions in a macromolecule. Another mechanism would be proposed which explains the nature of signals, for example, when the excitation is conducted through nerve fibrils–axons. However, in this case it is difficult to explain rather long relaxation times of these processes attaining several minutes and the fact that the same signals were recorded in the *in vitro* experiments with red and green uni–cellular algae and yeast cells.

The above–enumerated properties lead to a conclusion that a biological system, in particular, a living one, manifests nonlinear properties even on such weak levels of external excitation. For this reason the given systems, in our opinion, combined with perfect electronic means can serve as a very sensitive detector of weak excitations of various origin.

7. BIOLOGICAL DETECTOR DESIGNED FOR RECORDING OF WEAK COSMOPHYSICAL FIELDS

Biological objects can serve as sensitive detectors of weak signals of cosmic or any other origin. A large volume of reliable data on direct exposure of all kinds of fields on the living system and its response is now available. This response is variable in nature; however, it is important to know into what physical signals it transforms and how it is possible to record it most effectively with electronic devices.

A detector consisting of the above–mentioned permittivity meter and an active element is proposed for discussion. We have found that the most suitable active element is *blattella germanica*. This is due to two reasons. First, the object can be easily obtained. Second, its ability to keep alive appears to be very important for prolonged testing.

Its efficiency is illustrated by recording of total lunar eclipse. This event took place in the Far East on February 10, 1990. Figure 13 shows a record of this eclipse. The overshoots in the bell–shaped curve correspond to the same oscillations as shown in Fig. 10. The processes in this active element of biological detector caused by the impact of natural phenomena such as lunar eclipse have not been adequately determined yet. Hypothetically, we may assume that the exposure of variable gravitational field of the earth manifests in rearrangement of charge in macromolecules of the organism.

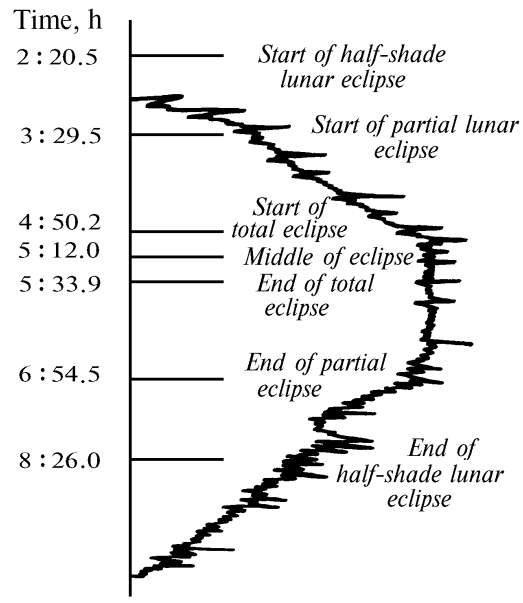

FIG. 13. Recording of lunar eclipse by means of measuring of permittivity of biological detector. Blattella germanica serves as an active element.

Comprehensive calculations of sensitivity of the detector can be performed for the cellular model of living organism proposed by Frelich.[30] In accordance with his ideas, electric interactions play an important role in the processes of life. They are manifested through electric dipoles formed in membranes of living cells which may be excited by metabolism and control over synthesis and division of cells. Further this model was improved by invoking of spontaneous avalanche processes powered by metabolic pumping. Under this assumption the macromolecules in membranes acquire electric dipole moments through avalanche process wherein potential metabolic energy is expended.

Processes which proceed simultaneously with macroscopic movements are caused by oscillations of specific structure of biological resonators initiating the required vital functions of the organism. After termination of current process macromolecules lose their activity until the next excitation. Rhythms of these processes are determined by the frequency of breathing and oscillations of natural and solar activities. The avalanche processes by themselves have their own dynamic parameters which may be changed under external excitation. Hence there are some important elements of the dynamics of living systems which have received sufficient study for their use in the detectors.

We went beyond a single testing of the detector. It was used in partial solar eclipse on July 10, 1991. The total solar eclipse was observed in Mexico. At present the obtained data are processed; however, preliminary results confirm the data obtained for lunar eclipse.[31,32]

In conclusion it should be noted that in the present paper we have described the results of joint experimental works without rigorous mathematical formulation of physical processes. First of all, this is connected with our wish not to encomber this material with "dry" mathematics; otherwise, this paper would be too tiring even for the most patient reader. In addition, an experiment can be always repeated or performed in a new way. In order to do this, we need no mathematical piles.

REFERENCES

1. D. Grischkowsky and S.R. Hartmann, Phys. Rev. Lett. **20**, No. 2, 41–43 (1968).
2. U.Kh. Kopvillem, V.N. Osipov, B.P. Smolyakov et al., Usp. Fiz. Nauk **105**, 767–769 (1971).
3. U.Kh. Kopvillem, Ukr. Fiz. Zh. **21**, No. 7, 1215–1217 (1976).
4. U.Kh. Kopvillem, Zh. Eksp. Tekh. Fiz. **42**, No. 5, 1333–1343 (1962).
5. U.Kh. Kopvillem, B.P. Smolyakov, and R.Z. Sharipov, Izv. Akad. Nauk SSSR ser. Fiz. **37**, 2240–2243 (1973).
6. Ya.Ya. Asadullin, U.Kh. Kopvillem, and V.N. Osipov, et al., Fiz. Tverd. Tela **13**, 2784–2786 (1971).
7. U.Kh. Kopvillem, B.P. Smolyakov, and R.Z. Sharipov, Pis'ma Zh. Eksp. Tekh. Fiz. **13**, 558–560 (1971).
8. B.P. Smolyakov, N.B. Angert, U.Kh. Kopvillem, et al., Fiz. Tverd. Tela **15**, 559–561 (1973).
9. B.P. Smolyakov, V.V. Samartsev, R.Z. Sharipov, et al., in: *Proceedings of the Sixth International Symposium on Nonlinear Acoustics*, Moscow (1975), Vol. 2, pp. 185–198.
10. I.E. Currie, T.A. Krumhanse, A.R. Bishop, et al., Phys. Rev. **B22**, No. 2, 477–497 (1980).
11. U.Kh. Kopvillem, B.P. Smolyakov, and R.Z. Sharipov, Phys. Lett. **A**, 1550–1554 (1973).
12. A.V. Alekseev, E.D. Kholodkevich, U.Kh. Kopvillem, et al., in: *Abstracts of Reports at the Eighth International Symp. Acoust.*, Leads (1981), p. 3.
13. Yu.E. Babanov, S.B. Zverev, and U.Kh. Kopvillem, in: *Abstracts of Reports at the All–Union Conference on Magnetic Resonance*, Kazan' (1984), Vol. 3, p. 73.
14. K.M. Salikhov, A.G. Semenov, and Yu.D. Tsvetkov, *Electron Spin Echo and its Application* (Nauka, Novosibirsk, 1976), 342 pp.
15. U.Kh. Kopvillem, B.P. Smolyakov, and R.Z. Sharipov, Fiz. Tverd. Tela **14**, No. 5, 1444–1447 (1972).
16. U.Kh. Kopvillem, B.P. Smolyakov, R.F. Khairov, et al., Radiospectrosk., No. 8, 3–7 (1974).
17. V.V. Samartsev, B.P. Smolyakov, R.F. Khairov, et al., in: *Acoustic Paramagnetic Resonance*, Kazan' (1975), pp. 97–122.
18. U.Kh. Kopvillem, and V.R. Nagibarov, Zh. Eksp. Tekh. Fiz. **54**, 312–316 (1968).
19. S.E. Kamenev, U.Kh. Kopvillem, A.S. Pasynkov, et al., Biofiz. **26**, 1051–1054 (1981).
20. S.E. Kamenev, U.Kh. Kopvillem, A.S. Pasynkov, et al., Ukr. Fiz. Zh. **26**, No. 11, 1911–1913 (1981).
21. A.S. Pasynkov, U.Kh. Kopvillem, and R.Z. Sharipov, Studia Biophysica **103**, No. 3, 225–229 (1984).
22. J.T. Gittleman, Y. Goldstein, and S. Bozowski, Phys. Rev. **B1**, 3609–3617 (1972).
23. R.Z. Sharipov and A.S. Burundukov, in: *Abstracts of Reports at the International School on Magnetic Resonance*, Novosibirsk (1987), p. 76.
24. R.Z. Sharipov and A.S. Burundukov, in: *Abstracts of Reports at the All–Union Conference on Application of Magnetic Resonance to National Economy*, Kazan' (1988), p. 112.
25. R.Z. Sharipov and A.S. Burundukov, in: *Abstracts of Reports at the 24th Congress: Ampere and Related Phenomena*, Poznan (1988), p. 38.
26. U.Kh. Kopvillem, R.Z. Sharipov, and A.S. Burundukov, in: *Abstracts of Reports at the 10th Meeting of the International Society of Magnetic Resonance*, Torino (1989), p. 6.
27. U.Kh. Kopvillem and R.Z. Sharipov, in: *Abstracts of Reports at the First Soviet–Chinese Symp. on Oceanography*, Vladivivostok (1990), p. 76.

28. U.Kh. Kopvillem and R.Z. Sharipov, in: *Proceedings of the Fourth All–Union Symp. on Atmospheric Electricity*, Nal'chik (1990), pp. 51–52.
29. R.Paul, V.A. Tuszunski, and R. Chatterju, Phys. Rev. **A30**, 2676–2685 (1984).
30. U.Kh. Kopvillem and R.Z. Sharipov, in: *Proceedings of the Second Symp. on Gravitational Waves and Gravitational Energy*, Dubna (1990), pp. 93–100.
31. U.Kh. Kopvillem and R.Z. Sharipov, in: *Proceedings of the Third Symp. on Gravitational Waves and Gravitational Energy*, Dubna (1991), pp. 62–69.
32. U.Kh. Kopvillem and R.Z. Sharipov, in: *Abstracts of Reports at the 12th Internartional Conference on Raman Spectr.*, South Carolina (1990), pp. 1–2.